Water Practice & Technology

IWA PUBLISHING

Water Practice & Technology Vol 18 No 12, 3280 doi: 10.2166/wpt.2023.201

Removal of methyl orange textile dye using magnetic chitosan microspheres adsorbent

Erik Estefan [a,b], Shinta Elystia [a,*], Wen-Hui Kuan [b] and Aryo Sasmita [a]

[a] Department of Environmental Engineering, University of Riau, Pekanbaru City, Indonesia
[b] Department of Safety, Health, and Environmental Engineering, Ming Chi University of Technology, New Taipei City, Chinese Taipei
*Corresponding author. E-mail: shinta.elystia@lecturer.unri.ac.id

EE, 0009-0001-3192-6784; SE, 0000-0002-8252-3299; W-HK, 0000-0003-1801-1763; AS, 0000-0002-5083-2994

ABSTRACT

Industrial textile wastewater contains high levels of dyes, which are potentially harmful to aquatic ecosystems by inhibiting sunlight penetration for photosynthesis activities. Adsorption is a simple method for pollutant removal for water treatment. Magnetic Chitosan Microspheres (MCM) has been developed as a natural adsorbent for dye removal. This study aimed to compare the properties of the raw adsorbent and after adsorption by FT-IR, BET, DLS, and SQUID Magnetometry. The adsorption behaviours were investigated by the influence of pH, contact time, and initial concentration on Methyl Orange removal. The result was MCM could eliminate MO until 93.60% at pH 7 with C0 100 mg L^{-1} in 5 min with an adsorption capacity of 187.21 mg g^{-1}. Adsorption processes were also studied through the isotherm and kinetic. The isotherm showed a closer fit to the Langmuir model than the Freundlich model. The kinetic result showed the PSO model was more suitable than PFO. The research data using MCM for adsorption demonstrated excellent adsorption capability in terms of dye removal percentage and high adsorption capacity. Therefore, this material could be an effective adsorbent for the treatment of dye-containing wastewater.

Key words: adsorption, artificial wastewater, chitosan, magnetic chitosan microspheres, magnetite, methyl orange

HIGHLIGHTS

- MO adsorption was studied using MCM.
- Properties of MCM were characterized with FT-IR, BET, DLS, and SQUID magnetometry.
- The percentage removal of MO dye using MCM was 93.60%.
- The adsorption process follows the Langmuir isotherm and pseudo-second-order (PSO) kinetic model.
- MCM showed faster MO removal and higher adsorption capacity when compared to other adsorbents.

1. INTRODUCTION

With the advancement of the world, the textile industry persistently expands, primarily due to the substantial demand for manufactured goods. The increase in textile production demand directly necessitates the use of dyes as an indispensable component in the dyeing process (Khoirudin 2015). In general, the textile industry predominantly employs synthetic dyes due to their numerous advantages, including ease of procurement, a wide range of available colours, practicality, convenience, as well as economic and cost-effectiveness (Kartina *et al.* 2013). During the dyeing process, approximately 10–15% of these dyes are discharged along with textile wastewater.

Methyl orange (MO), an azo dye with orange colour, is potentially harmful to aquatic ecosystems with its presence in the water environment. Although the toxicity is relatively low, its presence in water could inhibit the penetration of sunlight, thus affecting photosynthesis activities. Consequently leads to oxygen depletion in ecosystems and causes the death of aquatic organisms (Mahi 2021). Azo dyes recognized the threshold value in the water was 30 mg L^{-1}. Several methods have been employed to treat wastewater, such as coagulation (Liu *et al.* 2022), biological degradation (Ibrahim *et al.* 2022), and oxidation (Xu *et al.* 2022). However, technically treating wastewater containing dyes using these methods could be complex and costly (Yang *et al.* 2016).

Adsorption is a widely used method for wastewater treatment as it is considered economical and has no significant side effects (Rosema *et al.* 2021). Adsorption is also preferred over other methods due to its low initial cost, non-toxicity, high selectivity, and environmentally friendly (Kumari *et al.* 2017). The effectivity of adsorption is influenced by the adsorbent. As an alternative, one natural adsorbent that could be used is chitosan (Syahmani *et al.* 2017).

Chitosan is an organic biopolymer compound that is promising for adsorption application and is obtained from chitin through a deacetylation process. Chitosan contains reactive amino ($-NH_2$) and hydroxyl ($-OH$) groups within its structure and could be easily modified. The presence of amino groups in chitosan indicates its polycationic properties, while the hydroxyl groups indicate its hydrophilicity (Parlayici & Pehlivan 2021; Saheed *et al.* 2021). Chitosan has chemical and mechanical limitations such as forming a colloid on water, soluble in acid, having a small surface area, and being susceptible to biochemical and microbiological degradation (Amouzgar *et al.* 2016). To overcome these limitations, chitosan could be modified by the formation of composites with magnetite (Fe_3O_4).

Magnetite is a magnetic material that is suitable for adsorption processes due to its nanosized particles, which provide a large surface area, high adsorption capacity, and reusability. However, magnetite is prone to oxidation when exposed to air. The presence of chitosan could protect magnetite from its weaknesses and enhance its stability (Sharifi *et al.* 2021). Additionally, the adsorption capabilities of the combined materials are improved. Therefore, the composite of chitosan and magnetite could be a promising composite for wastewater treatment. However, there have been few works reported simultaneously for removing dyestuff from wastewater using this adsorbent. Yang *et al.* (2016) reported the adsorption of MO using the modified magnetic composite adsorbent, resulting in the removal of MO by 95%. Haldorai *et al.* (2015) also reported the MO adsorption using chitosan/Fe_3O_4 with the result of the removal of MO by 97%. Chen *et al.* (2020) also reported the magnetic chitosan biopolymer for removing the MO with a percentage of 93.5%.

In the current study, magnetic chitosan microspheres (MCM) were synthesized and developed as an effective adsorbent for the removal of MO from artificial wastewater. The properties of the adsorbent were examined under different characterization analyses, such as analysis of functional group by FT-IR, analysis of pore size and specific surface area by BET, analysis of particle size by DLS, and analysis of magnetic properties by SQUID, the results of the properties were compared between raw adsorbent and after adsorption. The adsorption process was also investigated under different experimental conditions, such as pH, contact time, and initial concentration were studied. Moreover, the equilibrium isotherms and kinetics of the adsorption process were also investigated.

2. MATERIALS AND METHODS

2.1. Chemicals

The chemicals and reagents used in this study, such as iron (III) chloride hexahydrate ($FeCl_3{\cdot}6H_2O$) was purchased from Thermo Fisher Scientific, iron (II) chloride tetrahydrate ($FeCl_2{\cdot}4H_2O$) was purchased from Alfa Aesar, chitosan (75–85% deacetylated) was purchased from Sigma-Aldrich, MO was purchased from Acros Organics, sodium hydroxide (NaOH) and hydrochloric acid (HCl) were purchased from Honeywell Fluka, ethanol was purchased from Echo Chemical, and acetone was purchased from Macron Fine Chemicals. All reagents were analytical reagent grade and used without further purification.

2.2. Instrumentation

Fourier transform infrared (FT-IR) spectra of the samples were obtained by PerkinElmer Spectrum One FT-IR Spectrometer in the range of 4,000 – 400 cm^{-1}. Specific surface area and pore size of MCM were measured by BET analysis using ASAP 2020. The particle size of the adsorbent was also measured by DLS analysis using Malvern Panalytical Zetasizer. The magnetic properties of MCM were detected by SQUID magnetometry using Quantum Design MPMS3. A spectrophotometer (Hach DR6000 UV/VIS Spectrophotometer), shaking bath, and freeze-drying vacuum were used in the experiment.

2.3. Preparation of MCM

MCM was prepared according to Yang *et al.* (2016) with slight modifications. MCM was synthesized by mixing 2.5 g of $FeCl_3{\cdot}6H_2O$ and 1.05 g of $FeCl_2{\cdot}4H_2O$ in 20 mL of deionized water. Subsequently, 50 mL of a chitosan solution (1 g in 50 mL of 1% HCl solution) was added. For 40 min, the solution was agitated vigorously, forming a yellow solution. After that, the solution was heated to 80 °C for 90 min under an N_2 atmosphere, followed by the

dropwise addition of 22 mL of 2 N NaOH solution, prompting a black precipitate. The precipitate was isolated from the solution with a neodymium magnet and washed several times with deionized water, ethanol, and acetone. The obtained precipitate was dried in a freeze-drying vacuum for 24 h. After the precipitate was dried, MCM was grounded in a mortar.

2.4. Adsorption experiments

The MO adsorption experiment was conducted in a batch experiment with some variation of different parameters, such as pH, contact time, and initial concentration. All the experiments were conducted in laboratory bottles with a capacity of 100 mL and then agitated at 250 rpm in a shaking bath and held for 1 h at 25 °C. After adsorption, the adsorbent with target dye was facilely isolated from the aqueous solution by using an external magnetic field, and the final concentrations of MO were measured with an absorption wavelength of 465 nm, respectively. The removal percentage (%) and the adsorption capacity of the MCM (q_e, mg g^{-1}) were determined by following the equations:

$$\% = \frac{(C_o - C_e)}{C_o} \times 100\,\% \tag{1}$$

$$q_e = \frac{(C_o - C_e)\,.\,V}{w} \tag{2}$$

where V is the volume of the solution (L) and w is the weight of adsorbents (g). C_o and C_e are the initial and equilibrium concentrations of MO in solution (mg L^{-1}), respectively.

The isotherm study was carried out with different initial concentrations of MO ranging from 50 to 250 mg L^{-1} while maintaining pH at 7 and contact time at 5 min. The isotherm study will be defined in two isotherm models, Langmuir and Freundlich isotherm model. The adsorption kinetic was studied for contact time ranging from 5 to 60 min by monitoring the adsorption capacity of MCM at each contact time. The kinetic study will be defined in two kinetic models, pseudo-first-order (PFO) and pseudo-second-order (PSO).

3. RESULTS AND DISCUSSION

3.1. Characterization of adsorbent

The FT-IR spectra of MCM before and after adsorption are shown in Figure 1. The MCM spectrum before adsorption showed the presence of peak absorption at wavelengths of 3,368, 1,622, 1,070, and 572 cm^{-1}. A peak

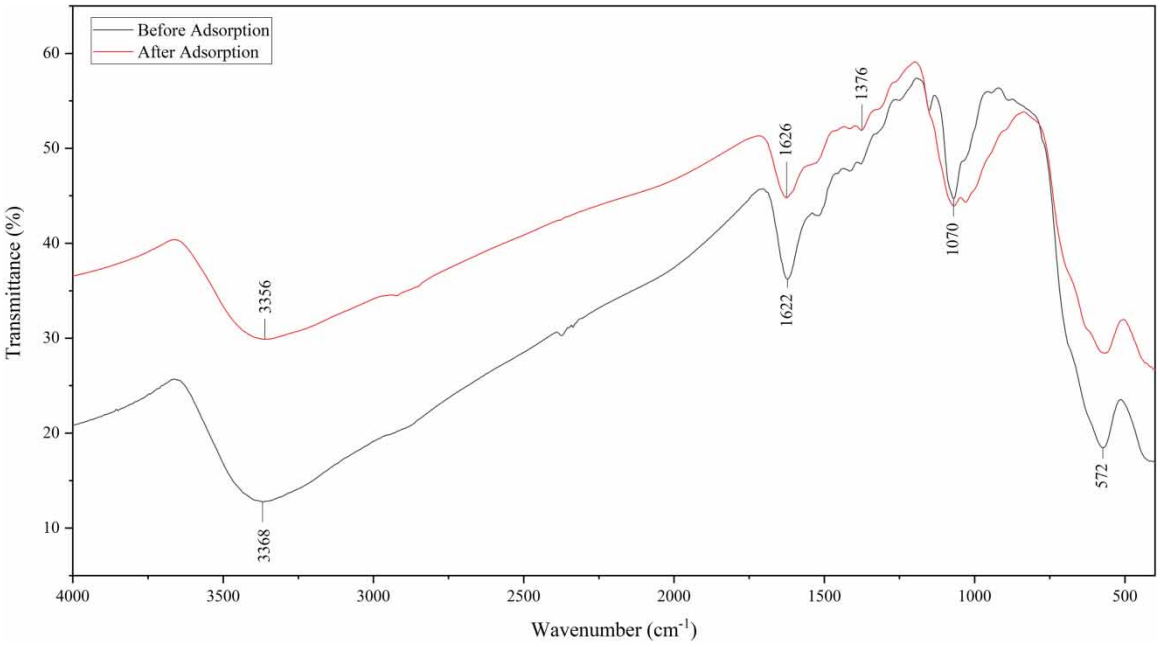

Figure 1 | FT-IR spectra of MCM before and after adsorption.

absorption at a wavelength of 3,368 cm^{-1} indicates the presence of a chitosan group from the stretching vibration of the –OH and –NH groups (Haldorai *et al.* 2015). The peak absorption at a wavelength of 1,622 cm^{-1} is associated with the stretching vibration at C–N and N–H, and at a wavelength of 1,070 cm^{-1} relates to the stretching vibration in C–O, which indicates that chitosan is successfully coated at Fe_3O_4 (Yang *et al.* 2016). The presence of Fe_3O_4 occurs at the peak absorption at a wavelength of 572 cm^{-1} with stretching vibration at the Fe–O bond. The FT-IR spectrum from MCM after adsorption shows shifts and decreases in intensity at 3,368–3,356 cm^{-1}, and 1,622–1,626 cm^{-1}, indicating the presence of binding to the dye molecule. In addition, the appearance of a new peak at the wavelength of 1,376 cm^{-1} indicates the presence of a $-SO_3^-$ group indicating the existence of the MO molecule on the surface of the adsorbent (Zhang *et al.* 2015). Also, the peak at the wavelength of 1,626 cm^{-1} indicates the presence of the stretching –N = N–, which is an azo group of MO (Acemioglu 2004).

The pore size and specific surface area of the MCM before and after the adsorption are shown in Table S1. Before adsorption, the pore size and specific surface area were 13.74 nm and 88.87 $m^2\ g^{-1}$. After adsorption, the pore size decreased by 56.77% to 5.74 nm. The surface area of the adsorbent also decreased by 44.39% to 49.42 $m^2\ g^{-1}$. This result indicates that the adsorption of MO on the pores and surface of the MCM, thereby reduces the pore size, as well as the surface area, while the adsorption process occurs.

The particle size of the MCM before adsorption was 447.3 nm. After the adsorption process, the MCM particle size increased by 51.45% to 677.3 nm. According to Yan *et al.* (2017), this suggests that agglomeration perhaps occurred during the adsorption which the adsorbed molecule binds to the surface of the adsorbent, also several particles attached to form an agglomerate.

The magnetic properties of MCM are shown in Figure 2. The magnetization saturation value of the MCM was 29.43 emu g^{-1}. This suggests that MCM exhibits a strong response to the magnetic field because its iron-containing material (Fe) has magnetic properties. Furthermore, no remanence coercivity was found indicating that MCM is superparamagnetic.

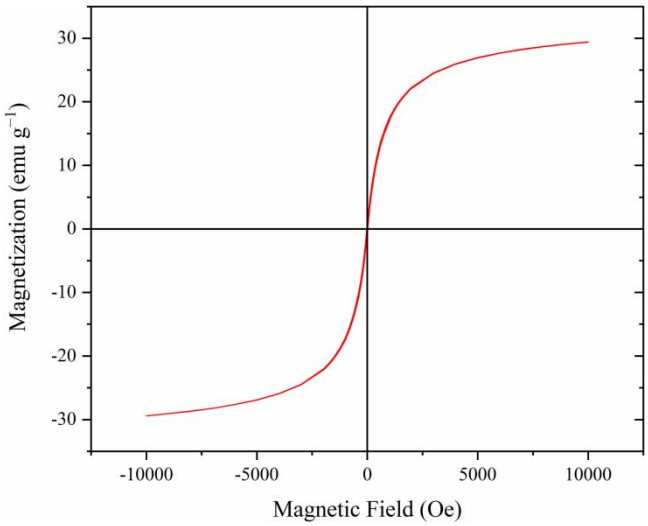

Figure 2 | Magnetization curves of MCM.

3.2. Effect of pH

The pH is one of the important parameters in the adsorption process because it affects chemical processes within the solution such as the activity of the functional group on adsorbents, ion competition, and the charges of the adsorbent surface. In addition, it could also affect adsorbent properties, adsorption mechanisms, and dissociation of adsorbed molecules (Rápó & Tonk 2021). In the study, the effect of pH was investigated in the range of 5–9 and adjusted with 0.1 N HCl or NaOH, and the results are illustrated in Figure 3. The removal of MO increased in the range of 5–7 and decreased at 8–9. In this work, the optimum pH was selected to be 7 with a removal percentage of 95.88%.

For pH values of 7 or higher (alkaline), the adsorption rate greatly increased, corresponding to the region where chemical adsorption occurs (Cruz-Lopes *et al.* 2021). According to Haldorai *et al.* (2015), the removal of dye may increase due to the electrostatic attraction between a negatively charged dye molecule with a positively charged adsorbent active site that becomes the main mechanism of the adsorption process. In addition,

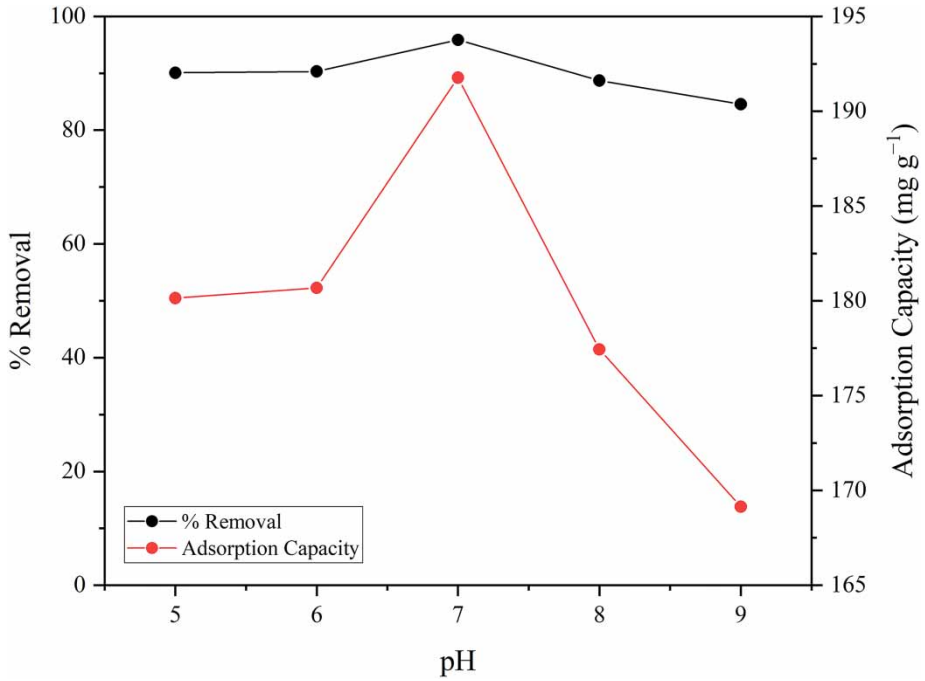

Figure 3 | Effect of pH on MO adsorption ($C_o = 100$ mg L^{-1}, dosage = 0.5 g L^{-1}, contact time = 45 min, shaking speed = 250 rpm).

the decrease of removal MO occurs because of the H^+ that caused the electrostatic repulsion with the active sites of the adsorbent and OH^- that competed with the dye molecule in binding with the adsorbent.

3.3. Effect of contact time

Contact time is an important parameter because, with a large percentage of removal of pollutants in a short time, it becomes an efficient adsorption process (Guo *et al.* 2021). In the study, the effect of contact time was investigated in the range of 5–60 min and the results are illustrated in Figure 4.

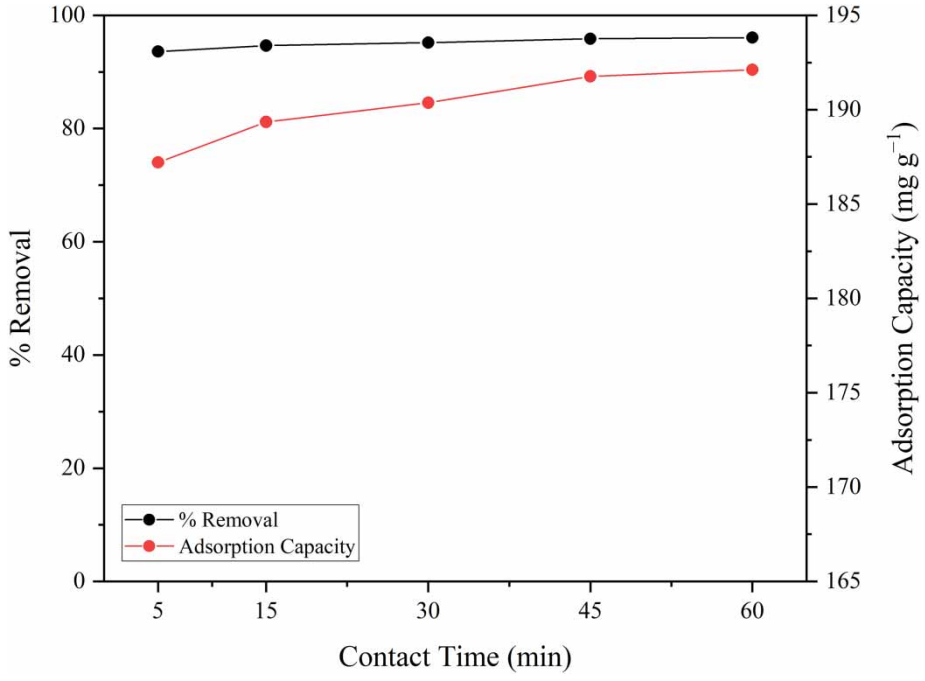

Figure 4 | Effect of contact time on MO adsorption ($C_o = 100$ mg L^{-1}, pH = 7, dosage = 0.5 g L^{-1}, shaking speed = 250 rpm).

The removal of MO increased as well as the longer contact time. This suggests that the longer the contact time of the adsorption between the dye and the adsorbent, the more dye could be adsorbed. According to Panda *et al.* (2017), the adsorption process appeared to proceed rapidly when the number of available sites was much larger than the number of adsorbates. Therefore, the optimum contact time is 60 min with percentage removal and adsorption capacity of 96.96% and 191.21 mg g^{-1}, respectively.

3.4. Effect of initial concentration

The initial concentration of adsorbents affects the removal efficiency by decreasing or increasing the availability of active sites on the surface of the adsorbent (Rápó & Tonk 2021). In the study, the effect of initial concentration was investigated in the range of 50–150 mg L^{-1} and the results are illustrated in Figure 5.

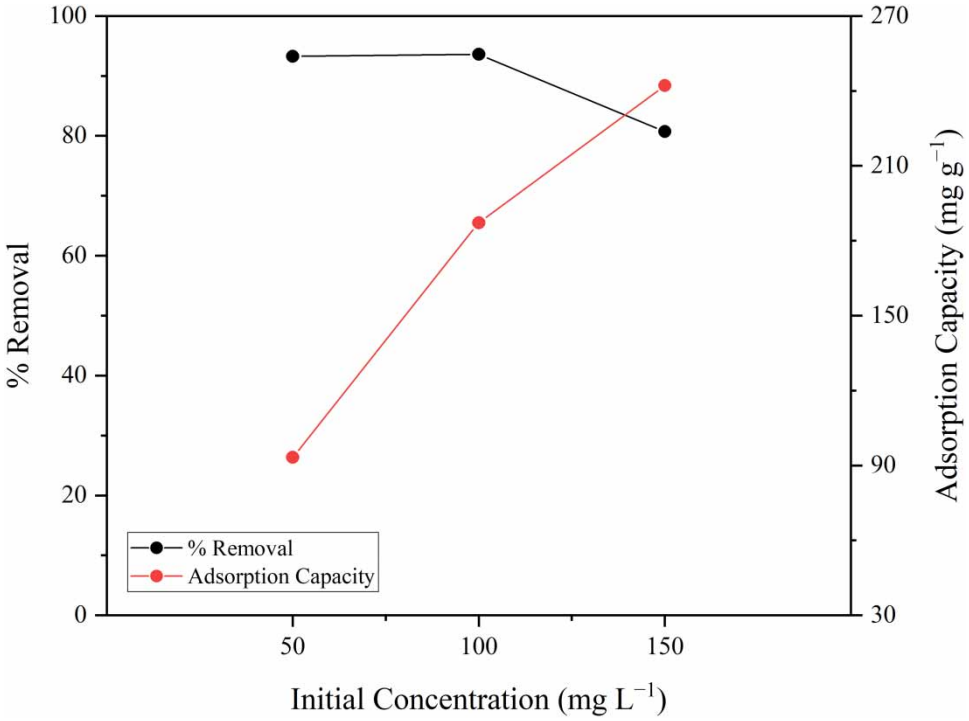

Figure 5 | Effect of initial concentration on MO adsorption (pH = 7, dosage = 0.5 g L^{-1}, contact time = 5 min, shaking speed = 250 rpm).

Figure 5 indicates that the equilibrium adsorption capacity of MO increases from 93.27 to 242.17 mg g^{-1} and the removal percentage decreases from 93.27 to 80.72%. According to Panda *et al.* (2017), in the case of low adsorbate concentrations, the ratio of the initial amount of adsorbate molecules to the available surface area of adsorbent is large and subsequently, the fractional adsorption becomes independent of the initial concentration. However, at higher concentrations, the available sites of adsorption become fewer, and hence the percentage removal of adsorbate which depends upon the initial concentration, decreases. Therefore, the optimum initial concentration on MO adsorption is 100 mg L^{-1} with a removal percentage of 93.60%.

3.5. Studies on adsorption mechanism

The adsorption mechanism of MO occurs by the influence of electrostatic interactions and hydrogen bonds. According to FT-IR spectra, the surface of MCM has some different functional groups such as –OH, –NH, C–N, N–H, C–O, and Fe–O groups. After the adsorption, FT-IR peaks move (3,368–3,356 cm^{-1}) in the direction of –OH and –NH groups were found in the spectra, indicating the presence of MO molecules binding to those groups. The surface of MCM was dominated by active sites ($-NH_2$ and $-OH$). Water molecules will present as dissociate agents into H^+ and OH^- ions. MO as R-SO_3Na will dissociate and release Na^+ ions, forming anionic dye ions ($R-SO_3^-$). While the active sites of MCM (–OH) will perform the adsorption process with hydrogen bond interaction. The oxygen atom of the S = O group from the sulphonate group ($-SO_3^-$) of MO could be used as

the hydrogen-bonding acceptor and formed intramolecular hydrogen bonding with the hydrogen atom of hydroxyl group (–OH) (Liu *et al.* 2019). Moreover, the active sites ($-NH_2$) will be protonated by H^+ ions, forming positively charged $-NH_3^+$. The adsorption process is performed through an electrostatic attraction of $R-SO_3^-$ from MO with active sites $-NH_3^+$ of MCM (Huang *et al.* 2017).

$$R-SO_3Na+H_2O \rightarrow R-SO_3^- + Na^+ \tag{3}$$

$$R-NH_3^+ + R-SO_3^- \rightarrow R-NH_3-O_3S-R \tag{4}$$

3.6. Studies on adsorption isotherm

The adsorption isotherm is generally studied through the isothermal approach to adsorption which is an important study for understanding an adsorbing process, in particular to know the number of adsorbed molecules that could be absorbed by a porous material. Two widely used isotherm models, Freundlich and Langmuir, were used in this work to examine the experimental data and assess the adsorption process on MCM. The Langmuir model assumes that the adsorbate forms a monolayer on the surface of the adsorbent, indicating chemical adsorption. The model could be represented by the following equation:

$$q_e = \frac{q_m K_L C_e}{1+K_L C_e} \tag{5}$$

where q_e and q_m represent the equilibrium and maximum adsorption capacities of adsorbate (mg g^{-1}), respectively; C_e represents the equilibrium concentration of solution (mg L^{-1}); and K_L represents a Langmuir constant concerning adsorption energy (L mg^{-1}). The Freundlich model assumes that the adsorbate forms a multilayer on the surface of the adsorbent, indicating physical adsorption. The model could be represented by the following equation:

$$q_e = K_F.C_e^{1/n} \tag{6}$$

where q_e represents the equilibrium adsorption capacity (mg g^{-1}); K_F and n represent the Freundlich constants, which were correlated with adsorption amount and adsorption intensity, respectively. The experimental data obtained from the variation of initial concentration were used to determine the appropriate isotherm model. The coefficient of determination (R^2) was used to determine the model that best fits the adsorption of MO using MCM, with a value closest to 1.

From the isotherm plotted in Figure 6, the isotherm parameters were obtained and shown in Table 1. These results indicate that the adsorption process of MO with MCM follows the Langmuir than the Freundlich adsorption mechanism, as the correlation coefficient approaches an R^2 value closer to 1 ($R = 0.9511$). Therefore, the adsorption process of MO with MCM occurs through chemical adsorption with monolayer-formed adsorbate on the surface of the MCM. The maximum adsorption capacity (q_m) was found to be 266.09 mg g^{-1}, calculated by Langmuir isotherm.

3.7. Studies on adsorption kinetic

The adsorption process could appear rapidly and control of the adsorption rate was arduous overall. However, there are often discrepancies in polarity between the adsorbate molecules at the surface of the adsorbent. Therefore, the time of binding of adsorbate molecules by the surface of the adsorbent becomes longer. The pseudo-first-order kinetic model is predicated on the assumption that the rate of adsorbate uptake per unit of time is directly proportional to the discrepancy in adsorption capacity and is typically well suited for characterizing the initial phase of an adsorption process. Additionally, the pseudo-first-order kinetic model is typically applicable in a system characterized by a high initial concentration of adsorbate and a limited number of active sites on the adsorbent. Equations are often used to describe liquid adsorption processes including PFO and PSO as given in the following equations.

$$q_t = q_e(1-e^{-k_1 t}) \tag{7}$$

$$q_t = \frac{k_2 q_e^2 t}{1+k_2 q_e t} \tag{8}$$

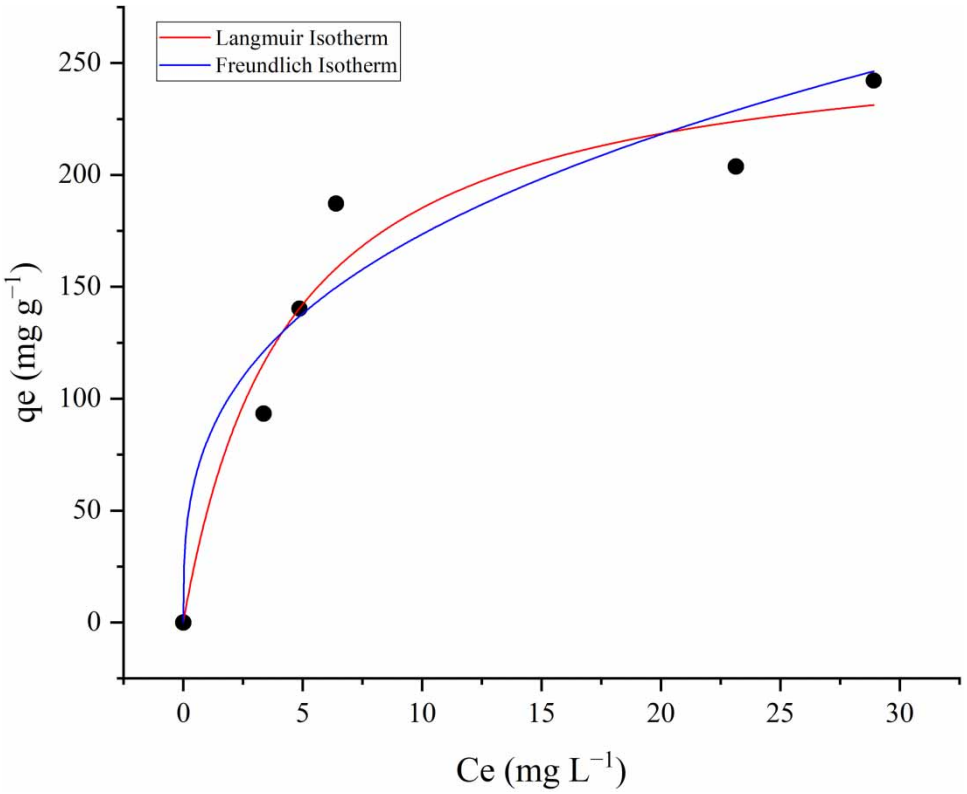

Figure 6 | Adsorption isotherm of MO by MCM (C_0 = 50–250 mg L^{-1}, pH = 7, dosage = 0.5 g L^{-1}, contact time = 5 min, shaking speed = 250 rpm).

Table 1 | Adsorption isotherm of MO by MCM

			Langmuir model			Freundlich model		
Adsorbate	**C_0 (mg L^{-1})**	**q_e (mg g^{-1})**	**q_m**	**K_L**	**R^2**	**K_F**	**n**	**R^2**
MO	50	93.27	266.09	0.229	0.9511	81.09	3.03	0.9489
	75	140.27						
	100	187.21						
	125	203.73						
	150	242.17						

where q_t and q_e represent the amount of adsorbate at time t (min) and the amount of adsorbate in equilibrium (mg g^{-1}), respectively, and k_1 and k_2 represent the equilibrium rate constant (min^{-1}).

From the kinetic plotted in Figure 7, the kinetic parameters were obtained and shown in Table 2. These results indicate that the kinetic adsorption process of MO with MCM is more suitable to the pseudo-second-order model, regarding the model showed a better correlation coefficient (R^2) with a value closer to 1 (R = 0.8811) with an equilibrium adsorption capacity of 191.838 mg g^{-1}. Therefore, the adsorption process of MO with MCM suggested that chemical adsorption might be the rate-determining step for controlling the adsorption process. Chemical adsorption occurs as a result of the abundance of active sites on the adsorbent and their interaction with the adsorbate through covalent bonding and electron exchange.

3.8. Comparison studies with other adsorbent

Table 3 presents some parameters compared to those of other adsorbents. The result shows that the MCM has a greater adsorption capacity and a shorter time for eliminating MO compared to the other materials. In addition, MCM could reach a maximum adsorption capacity of 266.09 mg g^{-1} within 5 min by calculation.

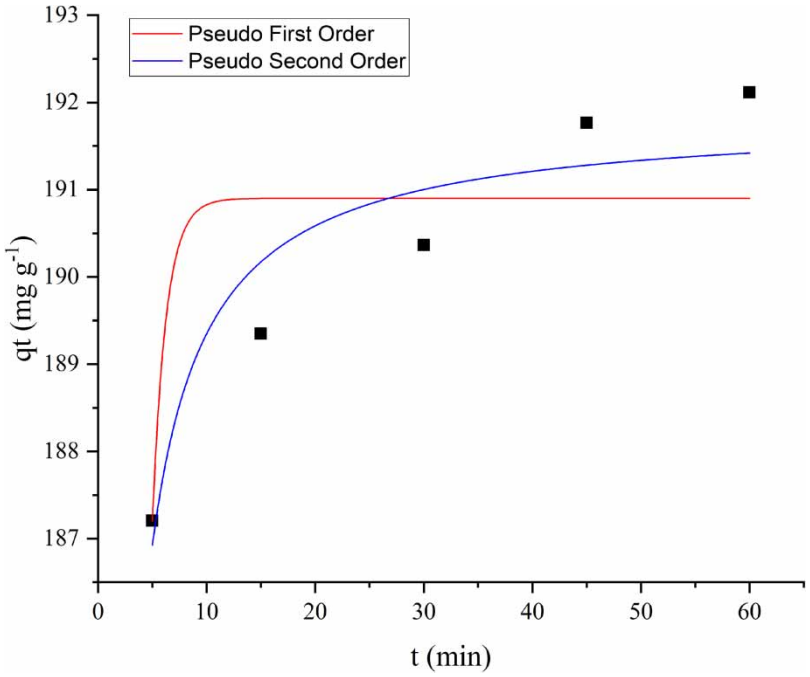

Figure 7 | Adsorption kinetic of MO by MCM ($t = 50$–250 min, pH = 7, dosage = 0.5 g L^{-1}, $C_0 = 100$ mg L^{-1}, shaking speed = 250 rpm).

Table 2 | Adsorption kinetic of MO by MCM

			Pseudo-first order (PFO)			Pseudo-second order (PSO)		
Adsorbate	***t* (min)**	**q_t (mg g^{-1})**	**q_e**	**k_1**	**R^2**	**q_e**	**k_2**	**R^2**
MO	5	187.205	190.899	0.788	0.6896	191.838	0.039	0.8811
	15	189.348						
	30	190.365						
	45	191.768						
	60	192.114						

Table 3 | Comparison with other adsorbent

Adsorbent	**q_m**	**Contact time**	**pH**	**References**
Glutaraldehyde cross-linking chitosan/fluorapatite-based natural phosphate composite	225.55	120 min	3	Billah *et al.* (2022)
Fe_2O_3–biochar nano-composite (Fe_2O_3–BC)	20.53	30 min	8	Chaukura *et al.* (2016)
Protonated cross-linked chitosan	89.3	12 h	6.7	Huang *et al.* (2017)
Fe_3O_4 nanoparticles functionalized activated carbon (Fe_3O_4/AC)	150.35	240 min	7	Liu *et al.* (2019)
Magnetic chitosan microspheres (MCM)	266.09	5 min	7	This study

3.9. Advantages of adsorption using magnetic adsorbent

The application of magnetic materials, which mainly consist of a magnetic core of iron oxides, organic compounds, carbon materials, etc., in the treatment of water has gained more interest in recent years. The separation of solid materials from liquid, which becomes increasingly difficult as particle size drops to the nanoscale, is the challenge that emerges in the use of these materials. On the other hand, the use of magnetic materials

is more effective and has the benefit of magnetic filtration in the separation of solid from liquid. Furthermore, compared to centrifugation or filtration, the removal of particles from solutions using magnetic fields is more efficient, effective, and frequently considerably faster. The advantages of using magnetic adsorbent for water treatment processes such as small size and thus high surface-to-volume ratio, solid/liquid separation through magnetic filtration is selective, faster than centrifugation and filtration techniques, reusability, greater biocompatibility, and magnetic separation (Sharma *et al.* 2018).

4. CONCLUSION

In this study, MCM was successfully synthesized and presented as a versatile adsorbent for dye wastewater. The adsorption experiment investigated the effect of pH, contact time, and initial concentration of MO. The optimum conditions were found on pH 7, 5 min of contact time, and an initial concentration of 100 mg L^{-1} with a removal percentage of 93.60%. The isotherm studies were performed by the Langmuir and Freundlich model. The result shows the maximum adsorption capacity from MO was 266.09 mg g^{-1} and the adsorption process of MO with MCM follows the adsorption mechanism of the Langmuir model with R^2 values of 0.9511. The kinetic studies were performed by PFO and PSO models. The result shows the adsorption process of MO with MCM follows the PSO model with R^2 values of 0.8811.

ACKNOWLEDGEMENTS

The work was supported by the University of Riau and Ming Chi University of Technology.

DATA AVAILABILITY STATEMENT

All relevant data are included in the paper or its Supplementary Information.

CONFLICT OF INTEREST

The authors declare there is no conflict.

REFERENCES

Acemioglu, B. 2004 Adsorption of Congo red from aqueous solution onto calcium-rich fly ash. *Journal of Colloid and Interface Science* **274**(2), 371–379.

Amouzgar, P., Wong, M. Y., Horri, B. A. & Salamatinia, B., 2016 Advanced material for pharmaceutical removal from wastewater. In: *Smart Materials for Waste Water Applications* (Mishra, A. K. ed.). Scrivener Publishing, Beverly.

Billah, R. E. K., Zaghloul, A., Ahsaine, H. A., Baqais, A., Khadoudi, I., El Messaoudi, N., Agunaou, M., Soufiane, A. & Jugade, R. 2022 Methyl orange adsorption studies on glutaraldehyde cross-linking chitosan/fluorapatite-based natural phosphate composite. *International Journal of Environmental Analytical Chemistry* **103**, 1–17.

Chaukura, N., Murimba, E. C. & Gwenzi, W. 2016 Synthesis, characterisation and methyl orange adsorption capacity of ferric oxide–biochar nano-composites derived from pulp and paper sludge. *Applied Water Science* **7**(5), 2175–2186.

Chen, B., Long, F., Chen, S., Cao, Y. & Pan, X. 2020 Magnetic chitosan biopolymer as a versatile adsorbent for simultaneous and synergistic removal of different sorts of dyestuffs from simulated wastewater. *Chemical Engineering Journal* **385**, 1–12.

Cruz-Lopes, L. P., Macena, M., Esteves, B. & Guiné, R. P. F. 2021 Ideal pH for the adsorption of metal ions Cr^{6+}, Ni^{2+}, Pb^{2+} in aqueous solution with different adsorbent materials. *Open Agriculture* **6**(1), 115–123.

Guo, T., Bulin, C., Ma, Z., Li, B., Zhang, Y., Zhang, B., Xing, R. & Ge, X. 2021 Mechanism of Cd(II) and Cu(II) adsorption onto few-layered magnetic graphene oxide as an efficient adsorbent. *ACS Omega* **6**(25), 16535–16545.

Haldorai, Y., Kharismadewi, D., Tuma, D. & Shim, J.-J. 2015 Properties of chitosan/magnetite nanoparticles composites for efficient dye adsorption and antibacterial agent. *Korean Journal of Chemical Engineering* **32**(8), 1688–1693.

Huang, R., Liu, Q., Huo, J. & Yang, B. 2017 Adsorption of methyl orange onto protonated cross-linked chitosan. *Arabian Journal of Chemistry* **10**(1), 24–32.

Ibrahim, A., El-Fakharany, E. M., Abu-Serie, M. M., Elkady, M. F. & Eltarahony, M. 2022 Methyl orange biodegradation by immobilized consortium microspheres: Experimental design approach, toxicity study and bioaugmentation potential. *Biology (Basel)* **11**(1), 1–27.

Kartina, B., Ashar, T. & Hasan, W. 2013 Karakteristik Pedagang, Sanitasi Pengolahan dan Analisa Kandungan Rhodamin B pada Bumbu Cabai Giling di Pasar Tradisional Kecamatan Medan Baru Tahun 2012 (Characteristics of traders, sanitation treatment and analysis of Rhodamine B content in grind chili seasoning at traditional markets in Medan Baru District on 2012). *Lingkungan dan Kesehatan Kerja* **1**, 1–7.

Khoirudin, M. 2015 *Biodegradasi Pewarna Tekstil Metil Orange oleh Jamur Pelapuk Coklat Gloephyllum trabeum (Biodegradation Metyhl Orange Textile Dye with Brown Decay Fungus Gloephyllum trabeum)*. Undergraduate Thesis, Faculty of Mathematics and Natural Science, Institut Teknologi Sepuluh Nopember.

Kumari, H. J., Krishnamoorthy, P., Arumugam, T. K., Radhakrishnan, S. & Vasudevan, D. 2017 An efficient removal of crystal violet dye from waste water by adsorption onto TLAC/Chitosan composite: A novel low cost adsorbent. *International Journal of Biological Macromolecules* **96**, 324–333.

Liu, X., Tian, J., Li, Y., Sun, N., Mi, S., Xie, Y. & Chen, Z. 2019 Enhanced dyes adsorption from wastewater via Fe_3O_4 nanoparticles functionalized activated carbon. *Journal of Hazardous Materials* **373**, 397–407.

Liu, Y., Xiang, Y., Xu, H. & Li, H. 2022 The reuse of nano-TiO_2 under different concentration of CO_3^{2-} – using coagulation process and its photocatalytic ability in treatment of methyl orange. *Separation and Purification Technology* **282**, 1–13.

Mahi, D. H. A. 2021 *Karakterisasi dan Adsorpsi Zat Warna Methyl Orange Menggunakan Zeolit Alam dengan Variasi Konsentrasi HCl (Characterization and Adsorption Methyl Orange Dye Using Natural Zeolite with Variation of HCl Concentration)*. *Undergraduate Thesis*, Faculty of Science and Technology, UIN Maulana Malik Ibrahim.

Panda, H., Tiadi, N., Mohanty, M. & Mohanty, C. R. 2017 Studies on adsorption behavior of an industrial waste for removal of chromium from aqueous solution. *South African Journal of Chemical Engineering* **23**, 132–138.

Parlayici, Ş. & Pehlivan, E., 2021 Modified Chitosan Forms for Cr (VI) Removal. In: *Chitin and Chitosan-Physicochemical Properties and Industrial Applications* (Berrada, M., ed.). IntechOpen, London, pp. 1–18.

Rápó, E. & Tonk, S. 2021 Factors affecting synthetic dye adsorption:desorption studies: A review of results from the last five years (2017–2021). *Molecules* **26**(17), 1–31.

Rosema, R., Supriyantini, E. & Sedjati, S. 2021 Pemanfaatan Kitosan untuk Menurunkan Kadar Logam Pb dalam Perairan yang Tercemar Minyak Bumi (Utilization of chitosan for decreasing Pb metal content in oil polluted waters). *Buletin Oseanografi Marina* **10**(1), 61–66.

Saheed, I. O., Oh, W. D. & Suah, F. B. M. 2021 Chitosan modifications for adsorption of pollutants – a review. *Journal of Hazardous Materials* **408**, 124889.

Sharifi, M. J., Nouralishahi, A., Hallajisani, A. & Askari, M. 2021 Magnetic chitosan nanocomposites as adsorbents in industrial wastewater treatment: A brief review. *Cellulose Chemistry and Technology* **55**, 185–205.

Sharma, M., Kalita, P., Senapati, K. K., Garg, A., 2018 Study on magnetic materials for removal of water pollutants. In: *Emerging Pollutants – Some Strategies for the Quality Preservation of Our Environment* (Soloneski, S. & Larramendy, M. L., eds). IntechOpen, London, pp. 61–78.

Syahmani, L., Iriani, R. & Sanjaya, R. E. 2017 Potency of Chitin as an adsorbent in black water treatment process at peatland environment. In: *1st International Conference on Social Sciences Education*, 3–4 November, Banjarmasin.

Xu, J., Ma, Q., Feng, W., Zhang, X., Lin, Q., You, C. & Wang, X. 2022 Removal of methyl orange from water by Fenton oxidation of magnetic coconut-clothed biochar. *RSC Advances* **12**(38), 24439–24446.

Yan, Y., Sun, K., Sun, Y., Zhang, Y., Guo, J., Deng, L. & Che, D. 2017 adsorption and agglomeration characteristics of ash particles after reducing flue gas temperature below the acid dew point. In *9th International Conference on Applied Energy*, 21–24 August, Cardiff.

Yang, D., Qiu, L. & Yang, Y. 2016 Efficient adsorption of methyl orange using a modified chitosan magnetic composite adsorbent. *Journal of Chemical & Engineering Data* **61**(11), 3933–3940.

Zhang, L., Hu, P., Wang, J., Liu, Q. & Huang, R. 2015 Adsorption of methyl orange (MO) by Zr (IV)-Immobilized cross-linked chitosan/bentonite composite. *International Journal of Biological Macromolecules* **81**, 818–827.

First received 22 August 2023; accepted in revised form 6 November 2023. Available online 16 November 2023